Bioorg. Med. Chem. 68 (2022) 116875

Contents lists available at ScienceDirect

Bioorganic & Medicinal Chemistry

journal homepage: www.elsevier.com/locate/bmc

Defined stereoisomers of 2″-amino NAD$^+$ and their activity against human sirtuins and a bacterial (ADP-ribosyl) transferase

Sarah Zähringer [a,b], Tobias Rumpf [b], Jelena Melesina [c], Alexander E. Lang [d], Klaus Aktories [d], Wolfgang Sippl [c], Manfred Jung [b], Gerd K. Wagner [e,*]

[a] Department of Chemistry, King's College London, Faculty of Natural & Mathematical Sciences, Britannia House, 7 Trinity Street, London SE1 1DB, United Kingdom
[b] Institute of Pharmaceutical Sciences, Albert-Ludwigs-University Freiburg, Albertstraße 25, 79104 Freiburg, Germany
[c] Institute of Pharmacy, Martin-Luther-University Halle-Wittenberg, Wolfgang-Langenbeck-Straße 4, 06120 Halle (Saale), Germany
[d] Institut für Experimentelle und Klinische Pharmakologie und Toxikologie, Faculty of Medicine, Albert-Ludwigs-Universität Freiburg, Albertstr 25, 79104 Freiburg, Germany
[e] School of Pharmacy, Queen's University Belfast, Medical Biology Centre, 97 Lisburn Road, Belfast BT9 7BL, United Kingdom

ARTICLE INFO

Keywords:
Nicotinamide adenine dinucleotide
Chemical tool
Stereochemistry
Sirtuin
ADP-ribosyltransferase

ABSTRACT

Nicotinamide adenine dinucleotide (NAD$^+$) is an important biomolecule with essential roles at the intersection of energy metabolism, epigenetic regulation and cell signalling. Synthetic analogues of NAD$^+$ are therefore of great interest as chemical tools for medicinal chemistry, chemical biology and drug discovery. Herein, we report the chemical synthesis and full analytical characterisation of three stereoisomers of 2″-amino NAD$^+$, and their biochemical evaluation against two classes of NAD$^+$-consuming enzymes: the human sirtuins 1–3, and the bacterial toxin TccC3. To rationalise the observed activities, molecular docking experiments were carried out with SIRT1 and SIRT2, which identified the correct orientation of the pyrophosphate linkage as a major determinant for activity in this series. These results, together with results from stability tests and a conformational analysis, allow, for the first time, a side-by-side comparison of the chemical and biochemical features, and analytical properties, of different 2″-amino NAD$^+$ stereoisomers. Our findings provide insight into the recognition of co-substrate analogues by sirtuins, and will greatly facilitate the application of these important NAD$^+$ analogues as chemical tool compounds for mechanistic studies with these as well as other NAD$^+$-dependent enyzmes.

1. Introduction

Synthetic analogues and derivatives of the enzyme co-factor nicotinamide adenine dinucleotide **1** (NAD$^+$, Fig. 1) are important chemical tool compounds for medicinal chemistry, chemical biology and drug discovery. Prominent examples include fluorescent derivatives for bioassays,[1,2] tagged derivatives for chemical proteomics,[3,4] and hydrolytically stable analogues for mechanistic and structural studies of NAD$^+$-dependent enzymes.[5] Such NAD$^+$-based probes are of particular interest for NAD$^+$-consuming enzymes that use **1** as a co-substrate for covalent modifications, such as lysine deacetylation and ADP-ribosylation reactions (Fig. 1).[6,7] Many of these NAD$^+$-consuming enzymes play a key role at the intersection of energy metabolism, epigenetic regulation and cell signalling, and represent established drug targets.[8–10]

Sirtuins are a class of NAD$^+$-dependent histone deacetylases that remove acetyl[11] as well as other acyl groups[12,13] from acylated lysines in histones and certain non-histone proteins. From bacteria to humans, sirtuins have been implicated in fundamental cellular processes, including transcriptional control,[14] metabolic regulation,[15] inflammation[16] and ageing.[17] They can also possess (ADP-ribosyl) transferase activity,[18] catalysing the transfer of ADP-ribose from **1** to an acceptor substrate. Although the catalytic mechanism of sirtuins is currently not fully understood, key steps have been identified.[5] These include the nucleophilic attack of the acyl group at position 1″ of the NAD$^+$ co-substrate, the formation of several mono- and bicyclic *O*-alkylamidates, and, ultimately, the release of the deacylated protein substrate (Scheme 1). For the formation of the intermediate *O*-alkylamidates, the 2″–OH group of **1** is crucial. Modifications of **1** in this position therefore offer an opportunity for the rational development of inhibitor candidates and mechanistic probes. However, only a limited number of

* Corresponding author.
E-mail address: g.wagner@qub.ac.uk (G.K. Wagner).

https://doi.org/10.1016/j.bmc.2022.116875
Received 31 March 2022; Received in revised form 31 May 2022; Accepted 31 May 2022
Available online 3 June 2022

examples for NAD^+ analogues with non-natural substituents in this position have previously been reported.[19,20]

Building on our previous work on the development of non-natural NAD^+ derivatives as chemical probes for NAD^+-consuming enzymes,[2,21,22] we recently became interested in the 2″-amino analogue of NAD^+ (Fig. 2). We hypothesized that the increased nucleophilicity of the 2″–NH_2 group may enable the trapping and identification of catalytic intermediates of the sirtuin mechanism. In principle, 2″-amino NAD^+ can exist as four main stereoisomers (Fig. 2), depending on the configuration at the anomeric position (α-/β-) and at position 2″ (*arabino*: **2**; *ribo*: **3**). While the synthesis and characterisation of 2″-amino *ara* NAD^+ (**2**) have been described,[19] to the best of our knowledge there is currently no published report of the chemical synthesis and analytical characterisation of 2″-amino *ribo* NAD^+ (**3**). The lack of these analytical and synthetic data is particularly striking as putative 2″-amino *ribo* NAD^+ **3** has been used in a stability study[23] and, separately, for the enzymatic synthesis of 2″–NH_2 cADPR.[24,25]

We have successfully synthesised three stereoisomers of 2″-amino NAD^+ (Fig. 2: **2**-β, **3**-α and **3**-β) including their full analytical characterization. All three stereoisomers were evaluated against two classes of mechanistically related NAD^+-consuming enzymes. Our results allow, for the first time, a direct, side-by-side comparison of the analytical properties and chemical and biochemical features of different 2″-amino NAD^+ stereoisomers. The analytical differentiation between these different isomers is not trivial, and their complete synthetic and analytical characterisation is therefore an essential prerequisite for applications of 2″-amino NAD^+ as a chemical tool compound. In particular, we provide a structural explanation for the differential stability of different isomers in this series. These differences have implications not only for the synthetic preparation and isolation of 2″-amino NAD^+ analogues, but also for the interpretation of their bioactivity. We have evaluated **2** and **3** as potential inhibitors of human sirtuins 1–3 (SIRT 1–3), and of a mechanistically related ADP-ribosyltransferase (ART), the bacterial toxin TccC3 from *Photorhabdus luminescens*. Interestingly, inhibitory activity against SIRT2 was largely independent of the stereochemistry of these 2″-amino NAD^+ analogues, whereas inhibition of TccC3 was only observed for the 2″-amino *ribo* NAD^+ **3**. Results from molecular docking experiments with SIRT1 and SIRT2 suggest that all 2″-amino NAD^+ analogues adopt a different hydrogen bonding pattern from the natural co-substrate NAD^+, which may explain their generally relatively modest activity. Taken together, our results provide new insights into the structural requirements for co-substrate recognition by these enzymes. They also provide, for the first time, an unambiguous structural basis for the interpretation of biological results with 2″-amino NAD^+, which will greatly facilitate its general application as a chemical tool compound in the future.

2. Results

Chemistry. 2″-Amino *ara* NAD^+ **2** (Fig. 2) was synthesized as previously reported.[19] The key step was the reduction of the corresponding 2″-azido precursor **4** with dithiothreitol (Scheme 2). Analysis of the crude reaction product by ^1H NMR suggested that **2** was formed in an α:β ratio of 1:5, in agreement with the literature.[19] However, after purification by anion-exchange chromatography, only the β-anomer of **2** was isolated, without any isolation of the corresponding α-anomer.

For the synthesis of the corresponding *ribo*-configured analogue 2″-amino *ribo* NAD^+ **3**, we adapted this general synthetic strategy (Schemes 3 & 4). The synthesis started with 3-azido-3-deoxy-1,2-*O*-isopropylidene-α-D-allofuranose **5**, which was prepared as described previously.[26] 4-Nitrobenzoylation of the primary alcohol followed by periodate cleavage gave the key intermediate **7** as a mixture of the 3-OH derivative and the corresponding 3-O-formyl derivative **7a** (Scheme 3).

Chlorination of **7a** with $TiCl_4$ and installation of the nicotinamide moiety under the conditions used for the preparation of the *arabino* configured analogue **2**[19] led exclusively to the attachment of the nicotinamide moiety in the α configuration (Scheme 4, 9-**α**). To achieve the attachment of the nicotinamide in the desired β configuration, alternative glycosylation conditions were therefore investigated. The use of $AgSbF_6$ as catalyst in combination with methanesulfonyl chloride as chlorination reagent as described by Cen et al. for the synthesis of 2″-substituted fluorine NAD^+ derivatives[20] enabled the attachment of the nicotinamide moiety in the desired β configuration (Scheme 4, 9-**β**).

The two anomers of **9** were obtained in a ratio of 1:1, in contrast to results in the *arabino* series, where the β-anomer of **2** was formed preferentially (Scheme 2). The mixture of **α/β** anomers of **9** was taken forward toward the synthesis of the corresponding 2″-amino NAD^+ **3**. For the pyrophosphate bond formation a Khorana-Moffatt procedure was chosen, which shortened the overall synthesis by three synthetic steps from the precursor 2′-azido *ribo* NMN **10** (Scheme 4), compared to the previous synthesis of Sleath and co-workers.[19] In the final step, the azido group was reduced to the corresponding amine with dithiothreitol as the reducing agent (Scheme 4). This step was accompanied by degradation of about 25% of the *trans*-configured 2″-amino NAD^+ analogue **3**-β, as detected by ^1H NMR. A similar level of degradation had also been observed during this step for **2**-α, the corresponding *trans*-configured analogue in the *arabino* series. The two anomers **3**-α and **3**-β were separated by semi-preparative HPLC and the stereochemistry was

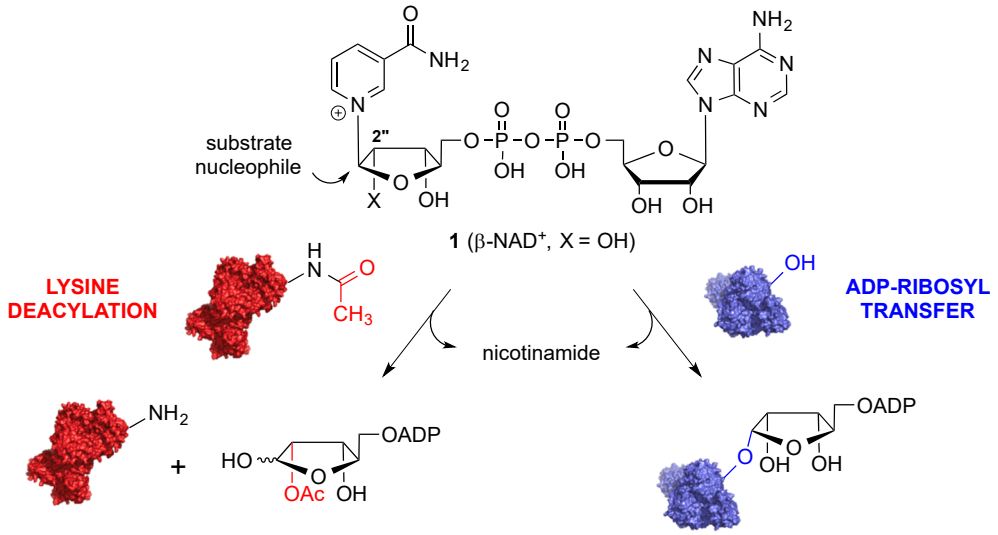

Figure 1. NAD^+ **1**, and its role as a co-substrate for enzymatic lysine deacylation and ADP-ribosyl transfer reactions.

established unambiguously by NOESY experiments (SI). The analysis of **3-**β showed a characteristic NOE correlation between H-1″ and H-4″ on the NMN ribose, indicating that these two protons are oriented on the same face of the ribose ring. This orientation of H-2″ was further confirmed by a NOE cross peak between H-2″ and H-6_N and between H-2″ and H-2_N. For the corresponding **3-**α analogue a NOE correlation was detected between H-4″ and H-2_N and between H-4″ and H-6_N.

Conformational analysis. In solution, **1** and its derivatives can exist in different conformations. The two predominant conformers differ in the orientation of the adenine base, which can be oriented either toward the ribose (*syn*) or away from it (*anti*) depending on the glycosyl torsion.[27,28] Information about the preferred conformation of NAD^+ derivatives can be extracted from ^{1}H NMR data. The chemical shift of the proton H-2′ in comparison with natural NAD^+, which exists predominantly in the anti confirmation, is an established indicator for the position of the *syn/anti* equilibrium.[27,28] H-2′ in natural NAD^+ resonates at 4.62 ppm and a downfield shift of this signal indicates a shift to the *syn* conformation. Using this approach, we analysed the preferred conformation of compounds **2**, **3** and **4** (Table 1). The H-2′ chemical shifts of these NAD^+ analogues are of the same order of magnitude as for natural NAD^+, which indicates that these NAD^+ analogues also adopt preferentially an *anti* conformation.

Stability tests. The substituent in position 2″ is adjacent to the labile nicotinamide riboside bond and may directly influence the chemical stability of these NAD^+ analogues.[23,29] Before evaluating their activity against our target enzymes, we therefore decided to experimentally determine the stability of both the α- and β-anomer of 2″–NH_2 *ribo* NAD^+ **3** in relevant media. For these stability tests, we established HPLC conditions that allowed the separation of the 2″-substituted NAD^+ analogues **3-**α and **3-**β from their cleavage products, i.e. the corresponding 2″-substituted ADPR derivative and nicotinamide. This was achieved using a Supelcosil™ RP-column and a potassium dihydrogen phosphate (KH_2PO_4) buffer at pH 6.0 against either methanol or acetonitrile (detection wavelength: 254 nm). Under these conditions, the NAD^+ analogues and nicotinamide were readily separated (SI, Fig. S1; t_R 2′’–NH_2 *ribo* β-NAD^+ = 14.6 min; t_R nicotinamide = 15.4 min). For the stability tests, a 1 mM solution of either 2″–NH_2 *ribo* α-NAD^+ **3-α** or 2″–NH_2 *ribo* β-NAD^+ **3-β** in sirtuin assay buffer (50 mM Tris/HCl, 137 mM NaCl, 2.7 mM KCl, pH 8.0) was incubated at 37 °C for 4 h. Samples were withdrawn at regular intervals (**3-α**: 60 min, **3-β**: 30 min) and analysed by HPLC (SI, Fig. S2). In order to allow a quantitative analysis, we established calibration curves for both nicotinamide and 2″–NH_2 NAD^+ (SI, Fig. S3). The concentration of nicotinamide was calculated by linear regression of the calibration curve and the percentage of cleaved nicotinamide in each sample at each time point was determined.

While both anomers showed some degradation under these conditions, 2″–NH_2 *ribo* NAD^+ **3-β** was less stable than the corresponding α-anomer (SI, Fig. S4). In the case of the β-anomer, 8% of nicotinamide were cleaved after 4 h of incubation, while for the α-anomer, only 4% of cleaved nicotinamide was observed (Table 2). The reduced stability of the β-anomer compared to the α-anomer is in agreement with the qualitative observations we made during the synthetic preparation of both anomers, specifically during the reduction of the azido group and the subsequent purification. We also repeated the stability experiments in the presence of the enzyme SIRT2, and the sirtuin substrate Z-(ε-acetyl)lysine-7-amino-4-methylcoumarin (ZMAL)[30] (SI, Fig. S5). Results under these conditions differed slightly from those in buffer alone. For the β-anomer, the cleavage of nicotinamide was increased in the presence of SIRT2 and ZMAL, compared to buffer alone, whereas no such difference was observed for the α-anomer (Table 2).

Biochemical results. The 2″-amino NAD^+ analogues **2** and **3**, as well as the 2″-azido NAD^+ analogue **4**, were tested as potential inhibitors of

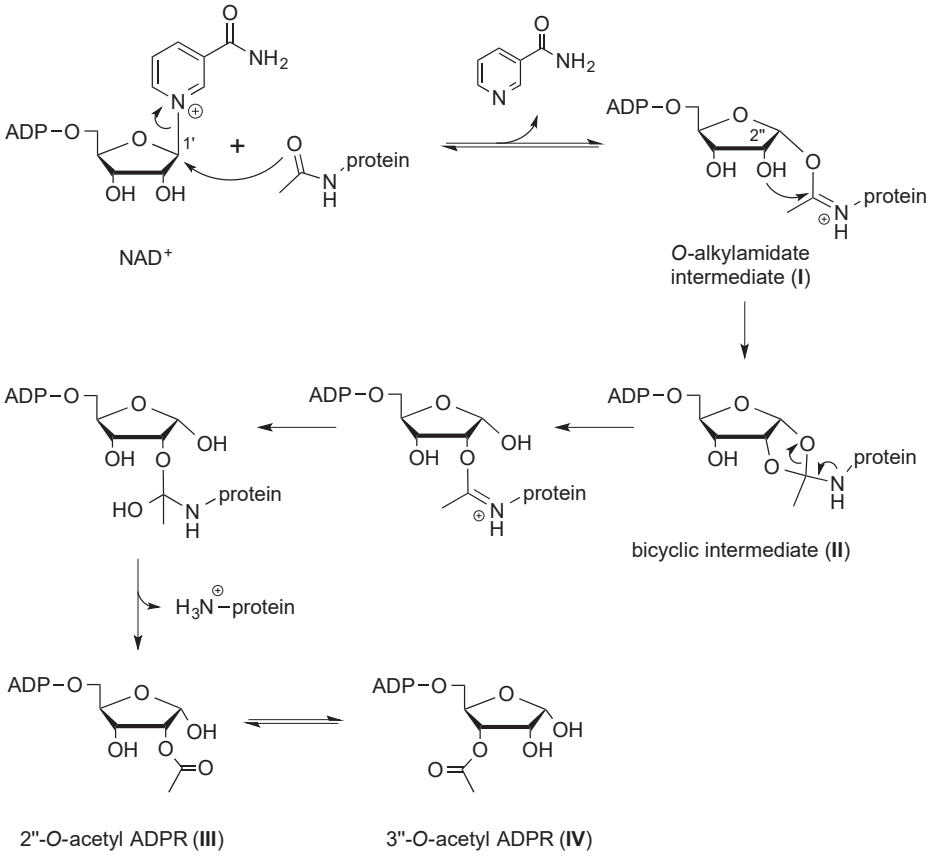

Scheme 1. Catalytic mechanism for the sirtuin-catalysed deacetylation of acetylated lysines in protein substrates (after Wang et al., *Cell Chem. Biol.* **2017**, 24, 339–345).

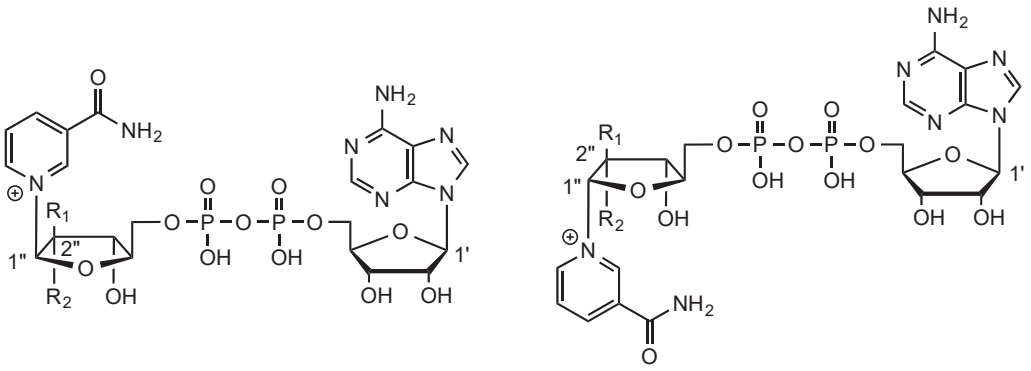

2-β: 2"-amino *ara* β-NAD$^+$ (R^1 = NH_2, R^2 = H) **2**-α: 2"-amino *ara* α-NAD$^+$ (R^1 = NH_2, R^2 = H)
3-β: 2"-amino *ribo* β-NAD$^+$ (R^1 = H, R^2 = NH_2) **3**-α: 2"-amino *ribo* α-NAD$^+$ (R^1 = H, R^2 = NH_2)

Figure 2. The different stereoisomers **2** and **3** of 2″-amino NAD$^+$.

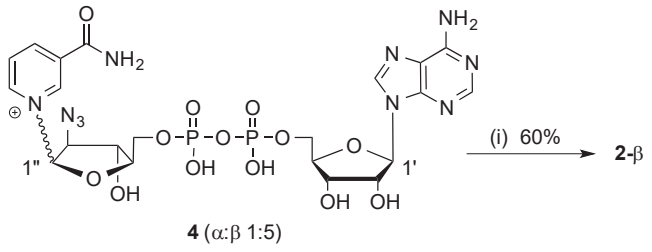

Scheme 2. Synthesis of 2″-amino *ara* NAD$^+$ **2** from the corresponding 2″-azido precursor **4**. *Reagents and conditions*: (i) DTT, H_2O, 0.1 M NaOH, rt, overnight. The ratio of **4**-α/**4**-β is based on ^{1}H NMR analysis. The reaction product was purified by anion-exchange chromatography and acidified to pH 2 with 0.1 M HNO_3 to give **2**-β as the sole anomer in 60% yield.

sirtuin isoforms 1–3. These experiments were carried out in an established bioassay, which is based on the sirtuin-mediated conversion of the fluorogenic, lysine-based substrate ZMAL to its deacetylated form ZML (SI, Scheme S1).[30] In principle, this assay can be used for the investigation of NAD$^+$ derivatives as either inhibitors (if added in the presence of NAD$^+$) or co-substrate analogues (if added instead of NAD$^+$). Upon co-incubation with NAD$^+$, the 2″-amino NAD$^+$ analogues showed modest inhibitory activity against SIRT2 and, to a lesser degree, against SIRT1, but no activity against SIRT3 (Table 3). While 2″-amino *ara* NAD$^+$ analogue **2-β** inhibited both SIRT1 and SIRT2 with IC_{50} values of about 150 μM, the corresponding 2″-azido analogue **4** was practically inactive against all three sirtuin isoforms tested (Table 3).

In principle, the 2″-amino NAD$^+$ analogues can behave as sirtuin substrates. To investigate this possibility, we repeated the assay with sirtuins 1–3 and 2″-amino NAD$^+$ analogue **3**-β instead of the natural cosubstrate NAD$^+$. Consumption of **3**-β in the sirtuin reaction would lead to the formation of 2″-*N*-acetyl ADP-ribose, corresponding to the 2″-*O*-acetyl ADP-ribose formed during the natural sirtuin mechanism, and hence to the standard assay signal (Scheme 1). However, no consumption of **3**-β by any of the three sirtuins was observed under these conditions, which suggests that this 2″-amino NAD$^+$ analogue is not accepted as a substrate by these sirtuins.

Finally, we also tested the 2″-amino NAD$^+$ analogues **2-β** and **3-β** as potential inhibitors of a bacterial ART, the toxin TccC3 from *Photorhabdus luminescens*.[31] TccC3 ADP-ribosylates actin in insects at threonine-148.[31] This modification prevents the interaction of actin with thymosin-β4 and leads to actin polymerization, a mechanism that is lethal for the insect.[31] An *in vitro* ADP-ribosylation assay with radioactive [^{32}P]NAD$^+$ (0.5 μCi per sample) and the ART domain of TccC3*hvr* from *Photorhabdus luminescens* was used to determine the ADP-ribosylation of α-actin. Proteins were detected by SDS-PAGE and the radiolabeled actin visualized by autoradiography (Fig. 3). The ADP-ribosylation of α-actin by TccC3*hvr* was measured in the presence of the potential inhibitors **2-β** and **3-β** at 10, 30 or 100 μM. These results show a concentration-dependent inhibition of ADP-ribosylation by 2″-amino *ribo* β-NAD$^+$ **3-β**, with 77% inhibition of ADP-ribosylation at the highest concentration tested (Fig. 3). In contrast, no inhibition was observed for the corresponding 2″-amino *ara* β-NAD$^+$ **2-β** (Fig. 3). This suggests that the configuration of the amino group in position 2″ plays a role for the inhibition of TccC3*hvr* by 2″-amino β-NAD$^+$ analogues.

3. Discussion

Our results show that the 2″-amino NAD$^+$ analogues **2** and **3** act as sirtuin inhibitors, albeit with relatively modest potency. All three stereoisomers showed a preference for SIRT2 over SIRT1, but were significantly less active against SIRT3. Surprisingly, **3-α** displayed the greatest activity in this series (IC_{50} 118 ± 5.4 μM against SIRT2), despite its different configuration at the anomeric centre of the nicotinamide riboside compared to the natural co-substrate β-NAD$^+$ (K_m 18 ± 3 μM for

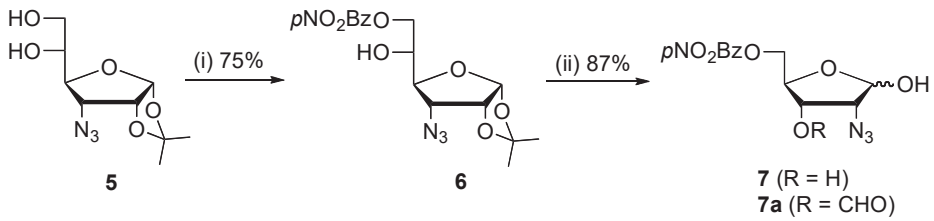

Scheme 3. Synthesis of 2-azido-2-deoxy-5-*O*-(*p*-nitrobenzoyl)-D-ribofuranose. *Reagents and conditionsReagents and conditions*: (i) *p*-nitrobenzoyl chloride, CH_2Cl_2, pyridine, −20 °C, 18 h; (ii) 50% TFA, rt, 48 h, then $NaIO_4$, $NaHCO_3$, acetonitrile, H_2O, rt, overnight. **7** and **7a** were separated by column chromatography ($CHCl_3$/ethyl acetate 2:1).

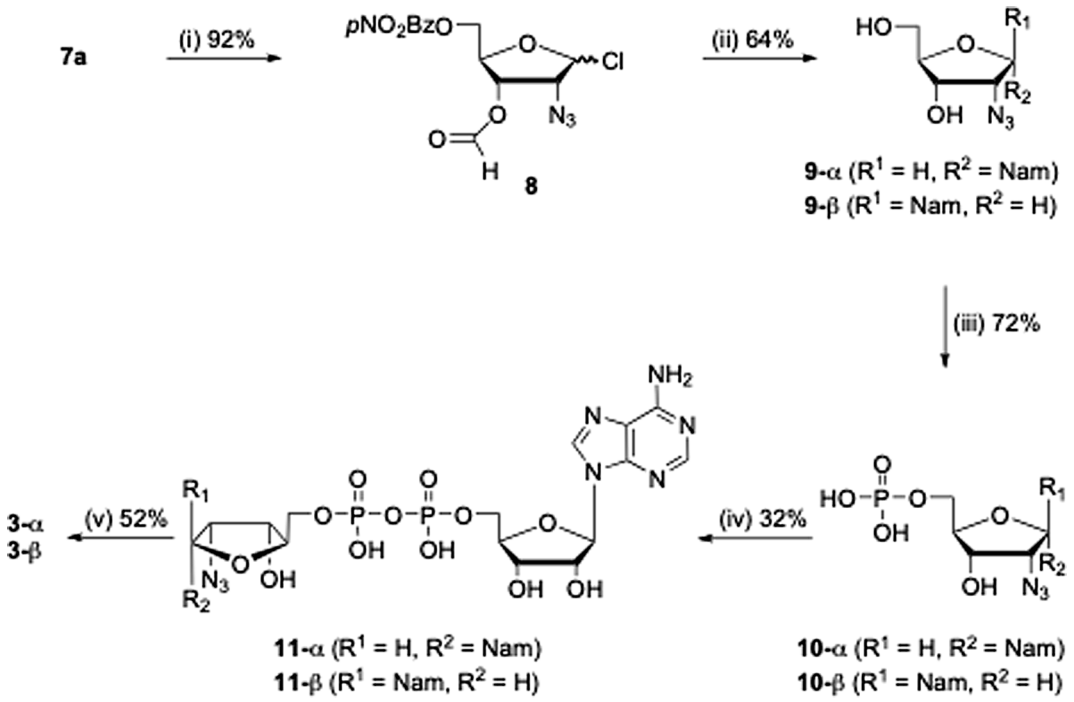

Scheme 4. Synthesis of 2″-amino *ribo* NAD$^+$ **3**. *Reagents and conditionsReagents and conditions*: (i) methanesulfonyl chloride, CH_2Cl_2, Et_3N. rt; (ii) nicotinamide, $AgSbF_6$, CH_2Cl_2, acetonitrile, rt, overnight; (iii) pyrophosphoryl chloride, *m*-cresol, 5 °C, overnight; (iv) AMP-morpholidate, $MgSO_4$, $MnCl_2$ in formamide, rt, overnight; (v) DTT, H_2O, 0.1 M NaOH, rt, overnight. **3**-α and **3**-β were separated by semi-preparative HPLC and the inorganic phosphate was removed by subsequent reverse-phase chromatography to give **3**-α (7.7 mg, 0.012 mmol) and **3**-β (10.0 mg, 0.015 mmol). Yields for **9**, **10**, **11** and **3** are combined yields of both anomers.

Table 1
Conformational analysis of 2″-substituted NAD$^+$ analogues **2**, **3** and **4**.

Compound	H-2′ (ppm)	ΔH-2′ (ppm)[1]	*syn/anti* orientation of the adenine base
2-β	4.66	0.04	anti
3-α	4.70	0.08	anti
3-β	4.72	0.10	anti
4-α	4.59	0.03	anti
4-β	4.67	0.05	anti

[1] ΔH-2′ values have been calculated as the difference between the chemical shift of H-2′ of the NAD$^+$ analogues, and H-2′ of β-NAD$^+$ (4.62 ppm).

Table 2
Cleavage of nicotinamide (Nam) from 2″-amino NAD$^+$ anomers **3**-α and **3**-β in the sirtuin assay buffer, with and without SIRT2/ZMAL.

Conditions	Compound	Cleaved Nam [%][1]
sirtuin buffer	**3**-α	4.1 ± 0.24
	3-β	8.4 ± 0.03
sirtuin buffer + SIRT2 + ZMAL	**3**-α	4.4; 4.1[2]
	3-β	15.1; 21.6[2]

[1] Percentage of cleaved Nam relative to the starting amount of NAD$^+$ analogue, after incubation for 4 h at 37 °C with and without SIRT2/ZMAL.
[2] Results from two separate experiments with different amounts of SIRT2.

SIRT2[32]).

To understand these results, we carried out molecular docking experiments with all three 2″-amino NAD$^+$ analogues and crystal structures of SIRT1[33] and SIRT2.[34] In both sirtuins, the β-NAD$^+$ co-substrate binds in a narrow, U-shaped channel (Fig. 4).[33,34] NAD$^+$ binding is stabilized by a large number of hydrogen bonds (SIRT1: 25 HBs; SIRT2: 24 HBs) involving the adenosine, pyrophosphate, and nicotinamide riboside moieties (Table 4). Molecular docking of **2-β**, **3-α** and **3-β** into the co-substrate binding site of SIRT1 indicates that despite the different stereochemistries, all three 2″-amino NAD$^+$ analogues can adopt the same overall orientation as NAD$^+$ (Fig. 4). Overlay of the docking solutions for **2-β**, **3-α** and **3-β** and NAD$^+$ shows excellent alignment of all four dinucleotides with regard to their adenosine and nicotinamide moieties (Fig. 4). Moreover, key interactions such as hydrogen bonding of the adenine ring to C482 and R466, and of the nicotinamide to I347 and D348, are preserved in all three 2″-amino NAD$^+$ analogues (ESI). In contrast, the orientation of the terminal ribose and, most significantly, the pyrophosphate linkage in **2-β**, **3-α** and **3-β** deviates substantially from that of NAD$^+$ (Fig. 4). Overall, the binding of all three 2″-amino NAD$^+$ analogues at SIRT1 involves significantly fewer hydrogen bonds than that of NAD$^+$ itself, especially in the region of the pyrophosphate linkage (Table 4). This "loss" of hydrogen bonds at the pyrophosphate linkage may therefore provide an explanation for the relatively modest activity of all three 2″-amino NAD$^+$ analogues against SIRT1.

A similar if more subtle trend was observed against SIRT2. Again, all three 2″-amino NAD$^+$ analogues engaged in fewer hydrogen bonds than NAD$^+$, but the drop was less significant than in the case of SIRT1, with a "loss" of only two hydrogen bonds (Table 4). In the case of **2-β** and **3-β**, the moiety that was most affected was once again the pyrophosphate linkage. In contrast, the most potent inhibitor in this series, **3-α**, formed the exact same number of hydrogen bonds at its pyrophosphate linkage as NAD$^+$ (Table 4).

Taken together, these results indicate that the observed activities against SIRT1 and SIRT2 in the 2″-amino NAD$^+$ series are driven by changes to the hydrogen bonding pattern. The observed preference of all three 2″-amino NAD$^+$ analogues for SIRT2 over SIRT1 can be explained by their capacity to better preserve the hydrogen bonding pattern of NAD$^+$ against SIRT2 than against SIRT1. The results with SIRT2 provide two intriguing insights: first, that a different stereochemistry at the terminal anomeric centre is not detrimental to activity, as evidenced by the superior activity of **3-α** over **2-β** and **3-β**, and second, that the most significant deviations from the hydrogen bonding pattern of NAD$^+$ concern not the nicotinamide riboside part, as could have been expected for a modification at the 2″-position, but the pyrophosphate linkage. SIRT2 appears capable of orienting the adenosine and nicotinamide

Table 3
Inhibition of sirtuin isoforms 1–3 by NAD^+ analogues **2**–**4.**

Code	Compound	IC_{50} (μM)[1]		
		Sirt1	Sirt2	Sirt3
2-β	2″–NH_2 *ara* NAD^+	176.2 ± 9.7	153.4 ± 10.1	47% @ 1 mM
3-α	2″–NH_2 *ribo* NAD^+	63% @ 250 μM 13% @ 100 μM	118 ± 5.4 μM	13% @ 250 μM 8% @ 100 μM
3-β	2″–NH_2 *ribo* NAD^+	65% @ 250 μM 18% @ 100 μM	151 ± 18.8 μM	19% @ 250 μM 12% @ 100 μM
4-α/-β	2″–N_3 *ara* NAD^+ (α:β 1:4)	n.i. @ 250 μM[2]	21% @ 250 μM n.i. @ 50 μM[2]	34% @ 250 μM n.i. @ 50 μM[2]

[1] Results are averages from 3 experiments. Inhibitors were initially tested at two concentrations only. IC_{50} values were determined for those inhibitors only that gave complete, or almost complete inhibition, at the highest concentration tested.
[2] No inhibition.

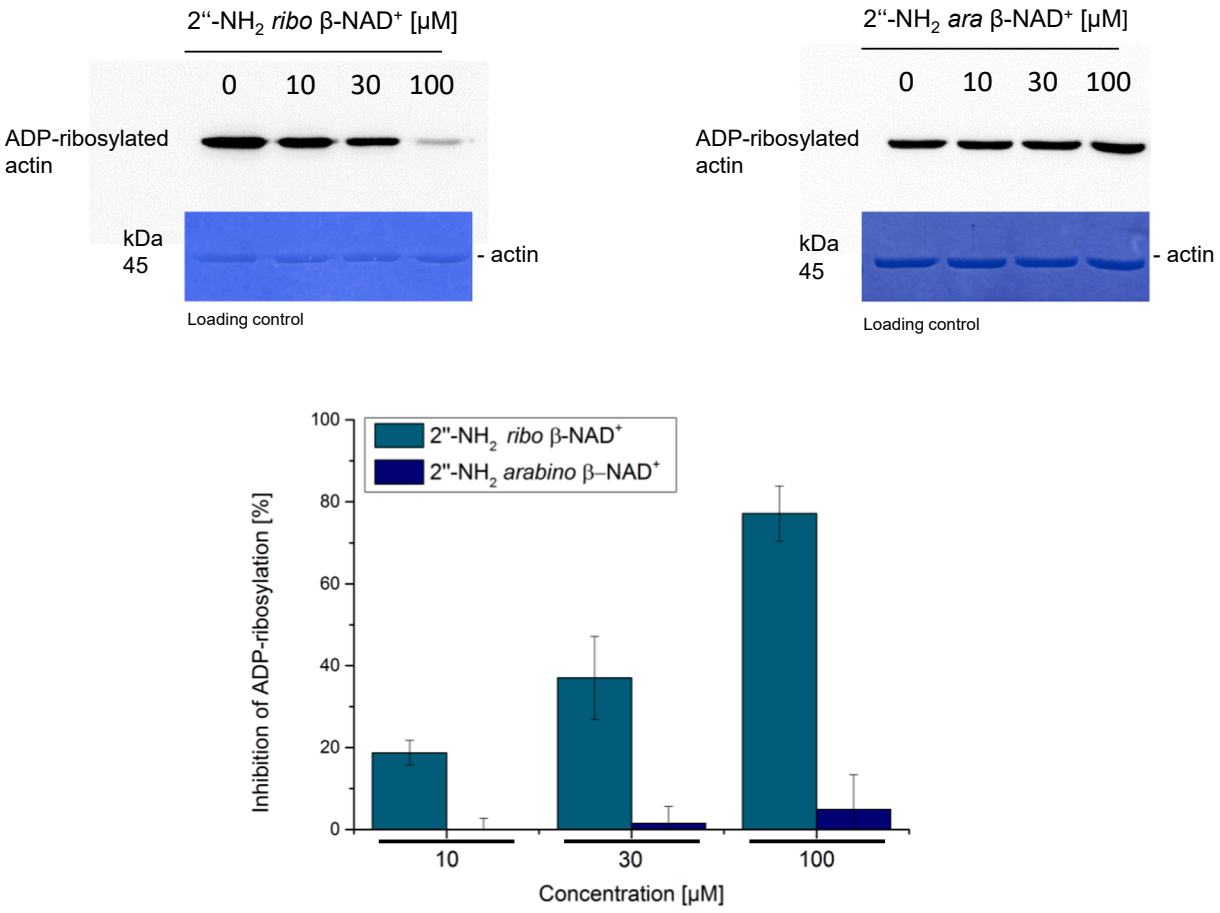

Figure 3. Effect of 2″-amino NAD^+ analogues **2-**β and **3-**β on *in vitro* ADP-ribosylation of α-actin by TccC3*hvr*. *Conditions*: 1 μM of α-actin was incubated with indicated concentrations of 2″–NH_2 *ribo* NAD^+ or 2″–NH_2 *arabino* NAD^+ for 15 min at 21 °C. Then, samples were subjected to an *in vitro* ADP-ribosylation assay with radioactive [^{32}P]NAD^+ (0.5 μCi per sample) and 70 nM of the ADP-ribosyltransferase domain of TccC3*hvr* from *Photorhabdus luminescens*. After 6 min at 21 °C, reaction was stopped by addition of SDS-containing Laemmli buffer and proteins were detected by SDS-PAGE and radiolabeled actin was visualized by autoradiography. The graph shows inhibition of ADP-ribosylation [%] compared to control.

moieties correctly in all three 2″-amino NAD^+ analogues, but only in the case of **3-α** does this also lead to a favourable orientation of the pyrophosphate linkage. This "long-range" effect of modifications at positions 1″ and 2″ of NAD^+ on the conformation, and recognition, of the pyrophosphate linkage has direct implications for the future design of NAD^+ analogues as molecular probes for sirtuins and related NAD^+-dependent enzymes.

Handlon and co-workers have reported a study on the chemical and enzymatic stability of NAD^+ derivatives with various substituents in position 2″, including 2″-amino *ribo* NAD^+ **3**.[23] However, neither the synthesis, nor any spectroscopic data in support of this structural assignment was included in this previous study.[23] Our results allow not only the unambiguous structural assignment of the different 2″-amino NAD^+ stereoisomers, but also a direct comparison of their chemical stabilities. Qualitative observations during the preparation of our target molecules show that within both the *ribo* and *arabino* series, the stereoisomers with the nicotinamide and 2″-amino groups in the *cis* orientation (**2-β**, **3-α**) are more stable than the corresponding *trans* isomers (**2-α**, **3-β**). Indeed, 2″-amino *ara* NAD^+ **2-α** was so unstable, that it could not be isolated during the synthesis.

The relative lack of stability of the *trans* isomers is directly related to the presence of the 2″-amino group. Degradation was observed only

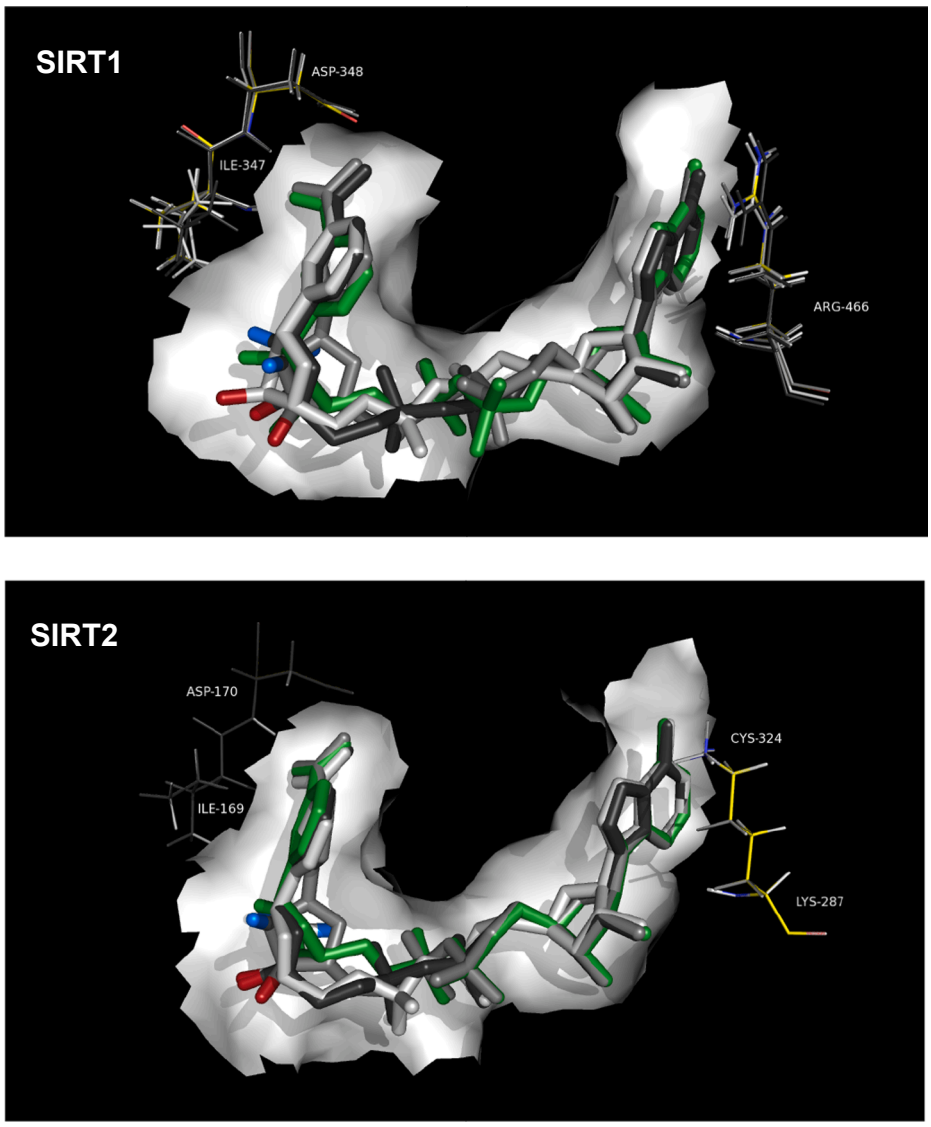

Figure 4. Overlay of molecular docking solutions for NAD^+ (green sticks) and the 2″-amino NAD^+ analogues **2-β** (black sticks), **3-α** (dark grey sticks) and **3-β** (light grey sticks) in the co-substrate binding site of SIRT1 and SIRT2. The 2″–NH_2 group in **2-β**, **3-α** and **3-β** is shown in blue, and the 3″–OH is shown in red. Key residues of the enzymes are shown in line representation. The surface of the binding pocket is shown in white.

Table 4
Hydrogen bond count for the interaction between SIRT1 and SIRT2, and NAD^+ or the 2″-amino NAD^+ analogues **2** and **3** (from molecular docking experiments). For a detailed list of individual interactions see the Supplementary Information.

(a) SIRT1

	adenosine	pyrophosphate	nicotinamide riboside	**total**
NAD^+	5	13	7	25
2-β	5	8	4	17
3-α	6	9	4	19
3-β	6	8	6	20

(b) SIRT2

	adenosine	pyrophosphate	nicotinamide riboside	**total**
NAD^+	9	10	5	24
2-β	9	8	5	22
3-α	8	10	4	22
3-β	8	8	6	22

upon reduction of the 2″-azido group to a 2″-amino group in the final step of the synthesis, while the 2″-azido analogues **4** and **11** displayed similar stability in both the *cis* and *trans* configuration. The combination of *trans* stereochemistry and 2″-amino group in the less stable isomers provides a possible mechanistic explanation for the degradation of the *trans* isomers **2-α** and **3-β**. Thus, a possible intramolecular nucleophilic attack of the amino group at the carbon in position 1″ may facilitate the cleavage of the nicotinamide leaving group. If the 2″-substituent is oriented *cis* to the nicotinamide leaving group, such an intramolecular nucleophilic attack is not possible due to geometrical constraints, and consequently these *cis* configured analogues are more stable.[29]

These qualitative observations were confirmed in the quantitative stability experiments with the *ribo* isomers **3-α** and **3-β**. In the assay buffer, the *trans* isomer **3-β** released twice as much nicotinamide than the *cis* isomer **3-α** (Table 2). This difference became even more pronounced upon addition of SIRT2 and the sirtuin substrate ZMAL to the stability experiment. The relative stability of the different 2″-amino *ribo* NAD^+ analogues is directly relevant for the interpretation of the sirtuin inhibition results, as the degradation product nicotinamide is itself known as a physiological sirtuin inhibitor.[35,36] Nicotinamide inhibits sirtuins through the so-called base-exchange pathway by rebinding to

the enzyme and accelerating the reverse reaction.[37,38] In the literature, IC_{50} values of 62–68 μM (against hSIRT1),[39,40] 34 μM (against hSIRT2),[38] and 37 μM (against hSIRT3)[40] have been reported. In our own assay, we have previously determined IC_{50} values for nicotinamide of 100 μM (against SIRT1) and 50 μM (against SIRT2). It could therefore be speculated that the inhibitory activities observed for the 2″-amino NAD^+ analogues **2-β**, **3-α** and **3-β** are, in fact, the result of the *in situ* release of nicotinamide. However, while nicotinamide inhibits all sirtuin isoforms, the 2″-amino NAD^+ analogues **2-β**, **3-α** and **3-β** show a clear preference for SIRT2. Moreover, if nicotinamide was the main inhibitory agent in our experiments, 2″-amino NAD^+ analogues that are less stable would be expected to be more active. This is not the case. Both **3-α** (more stable) and **3-β** (less stable) show similar inhibitory activity against SIRT2 (Table 2). While it cannot be ruled out that the release of nicotinamide may be a contributing factor to the sirtuin inhibition that was observed with our 2″-amino NAD^+ analogues, it is unlikely that this is the main mechanism.

4. Conclusion

We have synthesised NAD^+ analogues containing a 2″–NH_2 group instead of the 2″–OH group in the *arabino* and *ribo* configuration. In the natural cofactor β-NAD^+, the nicotinamide moiety is attached in the β configuration. We have prepared 2″–NH_2 *ribo* NAD^+ in both the α and β configuration and, for the first time, fully characterised both stereoisomers. The stereochemistry was unambiguously established by NOESY experiments.

Evaluation of the three 2″-amino NAD^+ analogues against three human sirtuins provided several insights into the recognition of co-substrate analogues by these enzymes. Our results suggest that even a relatively subtle modification such as the replacement of the 2″–OH with a 2″–NH_2 group leads to a drop in activity, compared to the parent dinucleotide. The modification is tolerated better by SIRT2 than by SIRT1, and least well by SIRT3, while a bulkier replacement such as the 2″-azido group is not tolerated well by any of the three sirtuins. Molecular docking experiments provide a possible structural rationale for these trends, indicating that the presence of the 2″-amino group may perturb the orientation of the pyrophosphate linkage. Unexpectedly, the anomeric stereochemistry did not seem to play a significant role for sirtuin inhibition, as both the *arabino* and *ribo* NAD^+ analogues **2** and **3** as well as the α and β anomers of **3** showed similar inhibition profiles. This is in contrast to results with another NAD^+-consuming enzyme, TccC3*hvr*. While compound **3**-β showed concentration-dependent inhibition of ADP-ribosylation of α-actin by TccC3*hvr*, no inhibition of this reaction was observed for its stereoisomer **2**-β.

These results provide intriguing clues about co-substrate recognition by different NAD^+-consuming enzymes. Modifications in the 2″-position of NAD^+ are of particular interest for the design of molecular probes for sirtuins, because of the involvement of the 2″-substituent in the sirtuin mechanism (ESI). Taken together with results from stability experiments, our findings will facilitate the design and the practical application of such probes.

5. Experimental section

5.1. General

All chemicals were obtained commercially and used as received unless stated otherwise. Anhydrous solvents sold on molecular sieves were used as such. Dichloromethane was dried over molecular sieves (4 Å) prior use. 2″–NH_2 *arabino* NAD^+ was synthesized, with minor modifications, as previously described.[19] TLC analysis was performed on precoated aluminium plates (silica gel 60 F_{254}, Merck). The identity of products was determined by ^1H, ^{13}C, and ^{31}P NMR spectroscopy and high resolution mass spectrometry (HRMS). The purity of tested compounds was determined by HPLC and met the required purity criteria (>95% by HPLC). NMR spectra were recorded on a Bruker Avance 400 spectrometer at 298 K. ^1H NMR spectra were recorded at 400 MHz, ^{13}C NMR spectra at 100 MHz and ^{31}P NMR spectra at 162 MHz or 202 MHz. Chemical shifts (δ) are reported in ppm and referred to D_2O, CD_3OD or $CDCl_3$ (respectively δ_H 4.79, 3.31, 7.26). Coupling constants are reported in Hz. Proton-signal assignments were made with aid of 2D ^1H–^1H NMR spectra (COSY). Stereochemical configuration was determined by NOE measurements. Accurate electrospray ionization mass spectra (HR ESI-MS) were obtained on a FinniganMAT 900 XLT mass spectrometer at the EPSRC National Mass Spectrometry Service Centre, Swansea, U.K. or on a LCQ-Advantage from ThermoElectron at the Institute for Organic Chemistry, Albert-Ludwigs-University, Freiburg. Preparative chromatography was performed on a Biologic LP chromatography system equipped with a peristaltic pump and a 254 nm UV optics module. HPLC analysis was carried out on an Agilent 1200 series equipped with a diode array detector and a Hichrom SAX column for semi-preparative HPLC or a Supelcosil RP 18 column for analytical purpose. 2-Azido-2-deoxy-5-*O*-(*p*-nitrobenzoyl)-D-ribofuranose (**7**) was synthesized according to the reported synthesis of 2″–NH_2 *arabino* NAD[19], starting from 1,2:5,6-di-*O*-isopropylidene-α-D-glucofuranose. The desired 2-azido-2-deoxy-5-*O*-(*p*-nitrobenzoyl)-D-ribofuranose (**7**) was separated by flash chromatography from 2-azido-2-deoxy-3-*O*-formyl-5-*O*-(*p*-nitrobenzoyl)-D-ribofuranose (**7a**) and used for the subsequent reaction.

5.2. Chemical synthesis

(*R*)-2-((3a*R*,5*S*,6*R*,6a*R*)-6-azido-2,2-dimethyltetrahydrofuro [2,3–d][1,3]dioxol-5-yl)-2-hydroxyethyl 4-nitrobenzoate (6). 5[26] (943 mg, 2.85 mmol) was dissolved in dichloromethane (7 mL) and pyridine (1.8 mL). The solution was cooled to −30 °C and *p*-nitrobenzoyl chloride (555 mg, 2.99 mmol) was added slowly. The reaction was stirred at −20 °C for 18 h. After cooling to room temperature, the solvents were evaporated and the residue was partitioned between toluene (20 mL) and water (20 mL). The aqueous phase was extracted with toluene (2 × 20 mL) and the combined organic layers were washed with water (3 × 20 mL) and concentrated in vacuo. The crude product was purified by column chromatography ($CHCl_3$/ether 3:1) to give **6** as a slightly yellow solid (843 mg, 2.14 mmol, 75%). ^1H NMR (400 MHz, $CDCl_3$) δ_H 8.25 (m, 4H, A_2B_2, *Ph* H-2,3,5,6), 5.83 (d, $J_{1,2} = 3.6$ Hz, 1H, H-1), 4.80 (apparent t, 1H, H-2), 4.54–4.52 (m, 2H, H-6_a, H-6_b), 4.31 (dd, $J = 4.7$, 10.7 Hz, 1H, H-5), 4.21 (dd, $J = 4.2$, 9.3 Hz, H-4), 3.65 (dd, $J = 4.7$, 9.3 Hz, 1H, H-3), 1.58 (s, 3H, CH_3), 1.37 (s, 3H, CH_3). ^{13}C NMR (100 MHz, $CDCl_3$) δ_C 164.7, 150.7, 135.0, 130.9, 123.6, 113.5, 104.2, 80.7, 80.4, 77.5, 69.3, 65.9, 60.1, 26.5, 26.4. *m/z* (ESI) 417.1017 $[M + Na]^+$, $C_{16}H_{18}N_4O_8Na$ requires 417.1017.

2-Azido-2-deoxy-5-*O*-(*p*-nitrobenzoyl)-D-ribofuranose (7). 6 (835 mg, 2.12 mmol) was dissolved in 35 mL 50% trifluoroacetic acid solution (water/dioxane/trifluoroacetic acid 1:1:2) and stirred at 25 °C. Reaction progress was monitored by TLC ($CHCl_3$/ether 2:1). After 48 h, all starting material had been consumed. Solvents were evaporated to give a brown solid, which was used without further purification. ^1H NMR analysis showed complete removal of the isopropylidene protecting group. The crude material was dissolved in acetonitrile (8 mL) and water (8 mL). Sodium bicarbonate (158 mg) and sodium periodate (499 mg, 2.33 mmol) were added, and the reaction mixture was stirred overnight at 25 °C. TLC analysis ($CHCl_3$/ethylacetate 2:1) showed two spots (*Rf*: 0.27 and 0.55) corresponding, respectively, to the desired product **7** and its 3-*O*-formyl derivative **7a**. The mixture was filtered, solvents evaporated, and the residue partitioned between water (20 mL) and ethylacetate (20 mL). The aqueous layer was washed with ethylacetate (2 × 20 mL) and the organic layers were combined, dried over $MgSO_4$, and evaporated. The mixture of **7** and its 3-*O*-formyl derivative **7a** was separated by flash chromatography ($CHCl_3$/ethylacetate 2:1) to give **7** as mixture of α- and β-anomer (α:β 2:3) in 47% yield, and **7a** as mixture of α- and β-anomer (α:β 1:2) in 40% yield.

7: ^{1}H NMR (400 MHz, $CDCl_3$, **7-α**) δ_H 8.31–8.17 (m, 4H, A_2B_2, *Ph* H-2,3,5,6), 5.55–5.52 (m, 1H, H-1), 4.66–4.45 (m, 3H, H-4, H-5$_a$, H-5$_b$), 4.28–4.31 (m, 1H, H-3), 3.87 (dd, J = 4.3, 5.4 Hz, 1H, H-2), 3.82 (OH), 2.93 (OH). ^{1}H NMR (400 MHz, $CDCl_3$, **7-β**) δ_H 8.31–8.17 (m, 4H, A_2B_2, *Ph* H-2,3,5,6), 5.40 (broad s, 1H, H-1), 4.66–4.45 (m, 3H, H-3, H-5$_a$, H-5$_b$), 4.22–4.18 (m, 1H, H-4), 4.02 (d, $J_{2,3}$ = 5.2 Hz, 1H, H-2), 3.45 (OH), 2.47 (OH). ^{13}C NMR (100 MHz, $CDCl_3$, **7-α**) δ_C 164.6 (q), 150.7 (q), 134.9 (q), 131.0 (Ar), 123.9 (Ar), 97.2 (CH), 82.0 (CH), 72.6 (CH), 65.0 (CH2), 63.8 (CH). ^{13}C NMR (100 MHz, CDCl3, **7-β**) δ_C 164.9 (q), 150.8 (q), 135.2 (q), 131.0 (Ar), 123.8 (Ar), 100.1 (CH), 81.0 (CH), 72.0 (CH), 67.8 (CH), 65.8 (CH_2). *m/z* (APCI) 342.1042 $[M + NH_4]^+$, $C_{12}H_{12}N_4O_7NH_4$ requires 342.1044.

7a: ^{1}H NMR (400 MHz, $CDCl_3$, **7a-α**) δ_H 8.24–8.11 (m, 5H, A_2B_2, *Ph* H-2,3,5,6, HC═O), 5.61 (d, $J_{1,2}$ = 4.2 Hz, 1H, H-1), 5.41 (dd, $J_{3,4}$ = 3.0 Hz, $J_{3,2}$ = 6.6 Hz, 1H, H-3), 4.62–4.43 (m, 3H, H-4, H-5$_a$, H-5$_b$), 3.88 (dd, $J_{2,1}$ = 4.3 Hz, $J_{2,3}$ = 6.5 Hz, 1H, H-2). ^{1}H NMR (400 MHz, $CDCl_3$, **7a-β**) δ_H 8.24–8.11 (m, 5H, A_2B_2, *Ph* H-2,3,5,6, HC═O), 5.55 (apparent t, 1H, H-3), 5.37 (broad s, 1H, H-1), 4.62–4.43 (m, 3H, H-4, H-5a, H-5b), 4.18 (dd, $J_{2,1}$ = 1.0 Hz, $J_{2,3}$ = 5.3 Hz, 1H, H-2). ^{13}C NMR (100 MHz, $CDCl_3$, **7a-α**) δ_C 164.4 (q), 160.2 (HC═O), 150.6 (q), 134.7 (q), 130.8 (Ar), 123.7 (Ar), 97.0 (CH), 79.7 (CH), 71.9 (CH), 64.4 (CH_2), 61.4 (CH). ^{13}C NMR (100 MHz, CDCl3, **7a-β**) δ_C 164.6 (q), 160.0 (HC═O), 150.7 (q), 134.9 (q), 130.9 (Ar), 123.6 (Ar), 100.6 (CH), 78.5 (CH), 72.8 (CH), 65.4 (CH), 65.3 (CH_2).

1-Chloro-2-azido-2-deoxy-3-*O*-formyl-5-*O*-(p-nitrobenzoyl)-D-ribofuranose (8). To a solution of **7a** (0.262 g, 0.74 mmol) in 5 mL anhydrous dichloromethane was added triethylamine (145 μL, 1.04 mmol) and the reaction was cooled to 0 °C under an atmosphere of nitrogen. Methanesulfonyl chloride (69 μL, 0.89 mmol) was added and the reaction mixture stirred at room temperature for 3 h under an atmosphere of nitrogen. The reaction mixture was evaporated and the residue dissolved in ethyl acetate (50 mL) and extracted with saturated $NaHCO_3$ (20 mL), 0.05 M HCl (20 mL) and water (20 mL). The organic layer was dried over Na_2SO_4, filtered and evaporated to give **8** as slightly yellow oil in 92% yield (0.254 g, 0.68 mmol) as a mixture of α- and β-anomer (α:β 3:4) that was used without separation in the following reaction. ^{1}H NMR (400 MHz, $CDCl_3$, **8**-β) δ_H 8.30–8.15 (m, 5H, HC═O, *Ph*), 6.07 (broad s, 1H, H-1), 5.76 (dd, J = 5.1, 7.8 Hz, 1H, H-3), 4.78–4.50 (m, 4H, H-2, H-4, H-5$_a$, H-5$_b$). ^{13}C NMR (100 MHz, $CDCl_3$, **8**-β) δ_C 164.3 (q), 159.7 (HC═O), 150.8 (q), 134.8 (q), 131.1 (Ar), 123.7 (Ar), 94.8 (C-1), 80.5 (C-4), 71.3 (C-3), 68.9 (C-2), 63.8 (C-5). ^{1}H NMR (400 MHz, $CDCl_3$, **8**-α) δ_H 8.30–8.15 (m, 5H, HC═O, *Ph*), 6.35 (d, J = 4.7 Hz, 1H, H-1), 5.48 (dd, J = 3.2, 7.3 Hz, 1H, H-3), 4.78–4.50 (m, 3H, H-4, H-5$_a$, H-5$_b$), 4.18 (dd, J = 4.7, 7.3 Hz, 1H, H-2). ^{13}C NMR (100 MHz, $CDCl_3$, **8**-α) δ_C 164.1 (q), 160.0 (HC═O), 150.9 (q), 134.6 (q), 130.9 (Ar), 123.9 (Ar), 94.9 (C-1), 82.9 (C-4), 70.4 (C-3), 63.7 (C-5), 63.3 (C-2).

1-(2′-Azido-2′-deoxy-D-ribofuranosyl)nicotinamide. (9). 8 (0.238 g, 0.64 mmol) and nicotinamide (0.196 g, 1.61 mmol) were dissolved in 7 mL anhydrous dichloromethane under an atmosphere of nitrogen. Another 2.5 equivalents nicotinamide (0.196 g, 1.61 mmol) and $AgSbF_6$ (0.221 mg, 0.64 mmol) were dissolved in 15 mL anhydrous acetonitrile and added to the reaction at 0 °C. The resulting reaction mixture was left stirring overnight at room temperature under nitrogen atmosphere. The reaction was evaporated to dryness in vacuo. After addition of methanol the suspension was filtered through celite and evaporated.

For the following deprotection step, 5 mL of 7 N methanolic ammonia were added and the reaction was stirred for 4 h at 0 °C. The crude product was concentrated in vacuo, dissolved in a minimum amount of methanol and precipitated with cold ether (2x) to give a brown solid, which was purified by reverse-phase chromatography to remove residual nicotinamide (5–80% acetonitrile against H_2O over 300 mL, flow rate: 3 mL/min). The product **9** was obtained in 64% yield (0.130 g mg, 0.41 mmol) as mixture of α- and β-anomer (α:β 1:1) that was used without separation in the following reaction. ^{1}H NMR (400 MHz, D_2O, **9**-β) δ_H 9.64 (s, 1H, H-2$_N$), 9.29 (d, J = 6.5 Hz, 1H, H-6$_N$), 8.97 (d, J = 8.0 Hz, 1H, H-4$_N$), 8.26 (dd, J = 6.5, 8.0 Hz, 1H, H-5$_N$), 6.27 (d, J = 3.4 Hz, 1H, H-1′), 4.65–4.61 (m, 2H, H-2‘, H-3′), 4.45–4.43 (m, 1H, H-4′) 4.06 (dd, J = 2.7, 13.0 Hz, 1H, H-5$_a$′), 3.92–3.90 (m, 1H, H-5$_b$′). ^{13}C NMR (100 MHz, D_2O, **9**-β) δ_C 145.9 (C-4$_N$), 142.8 (C-6$_N$), 140.7 (C-2$_N$), 132.8 (q), 128.4 (C-5$_N$), 98.2 (C-1′), 87.5 (C-4′), 69.9 (C-3′), 68.2 (C-2′), 59.6 (C-5′). NOESY (**9**-β): NOE correlation observed between H-1′ and H-4′. ^{1}H NMR (400 MHz, D_2O, **9**-α) δ_H 9.29 (s, 1H, H-2$_N$), 9.08 (d, J = 6.5 Hz, 1H, H-6$_N$), 8.95 (d, J = 8.0 Hz, 1H, H-4$_N$), 8.20 (dd, J = 6.5, 8.0 Hz, 1H, H-5$_N$), 6.65 (d, J = 5.8 Hz, 1H, H-1′), 5.01 (apparent t, 1H, H-2′), H-4′ under water peak, 4.65–4.63 (m, 1H, H-3′), 3.91 (dd, J = 3.1, 12.9 Hz, H-5$_a$′), 3.78 (dd, J = 4.2, 12.9 Hz, 1H, H-5$_b$′). ^{13}C NMR (100 MHz, D_2O, **9**-α) δ_C 145.5 (C-4$_N$), 143.5 (C-6$_N$), 141.1 (C-2$_N$), 134.0 (q), 127.2 (C-5$_N$), 95.6 (C-1′), 88.9 (C-4′), 70.9 (C-3′), 64.5 (C-2′), 60.7 (C-5′). NOESY (**9**-α): NOE correlation identified between H-1′ and H-3′. *m/z* (ESI, α and β mixture) 280.1045 $[M]^+$, $C_{11}H_{14}N_5O_4$ requires 280.1040.

2′-Azido-2′-deoxy-ribonicotinamide mononucleotide (10). All glassware was dried in an oven at 200 °C overnight before use. **9** (0.039 g, 0.14 mmol, freeze dried material) was dissolved in 5 mL *m*-cresol and cooled to 5 °C. Pyrophosphoryl chloride (88 μL, 0.55 mmol) was added and the reaction mixture stirred overnight at 5 °C under an atmosphere of nitrogen. The reaction was quenched by addition of ice-water (30 mL) and extracted with diethyl ether to remove the *m*-cresol. The aqueous layer was evaporated to dryness in vacuo and re-dissolved in a minimum amount of methanol and precipitated with ice-cold acetone. The precipitate was purified by ion exchange chromatography to give product **10** in 61% combined yield of both anomers (0.035 g, 0.58 equiv. Et_3N, 0.085 mmol). ^{1}H NMR (400 MHz, D_2O, **10**-β) δ_H 9.54 (s, 1H, H-2$_N$), 9.33 (d, J = 6.5 Hz, 1H, H-6$_N$), 8.99 (d, J = 8.0 Hz, 1H, H-4$_N$), 8.29 (t, J = 6.5, 8.0 Hz, 1H, H-5$_N$), 6.21 (d, J = 5.2 Hz, 1H, H-1′), H-2′, H-3′ under water peak, 4.62–4.59 (m, 1H, H-4′), 4.27–4.23 (m, 1H, H-5$_a$′), 4.08–3.99 (m, 1H, H-5$_b$′). ^{13}C NMR (100 MHz, D_2O, **10**-β) δ_C 146.3 (C-4$_N$), 142.6 (C-6$_N$), 140.1 (C-2$_N$), 128.6 (C-5$_N$), 98.3 (C-1′), 87.4 (C-4′), 70.9 (C-3′), 68.3 (C-2′), 63.9 (C-5′). ^{31}P NMR (162 MHz, D_2O, **10**-β) δ_P 3.47 (s). NOESY (**10**-β): NOE correlation identified between H-1′ and H-4′. ^{1}H NMR (400 MHz, D_2O, **10**-α) δ_H 9.32 (s, 1H, H-2$_N$), 9.10 (d, J = 6.5 Hz, 1H, H-6$_N$), 8.94 (d, J = 8.0 Hz, 1H, H-4$_N$), 8.19 (dd, J = 6.5, 8.0 Hz, 1H, H-5$_N$), 6.68 (d, J = 6.1 Hz, 1H, H-1′), 5.14 (apparent t, 1H, H-2′), 4.95–4.91 (m, 1H, H-4′), 4.74–4.72 (m, 1H, H-3′), 4.09–3.99 (m, 2H, H-5$_{a,b}$′). ^{13}C NMR (100 MHz, D_2O, **10**-α) δ_C 145.5 (C-4$_N$), 143.6 (C-6$_N$), 141.1 (C-2$_N$), 127.1 (C-5$_N$), 95.8 (C-1′), 87.8 (C-4′), 71.0 (C-3′), 64.5 (C-5′), 64.3 (C-2′). ^{31}P NMR (162 MHz, D_2O, **10**-α) δ_P 3.78 (s). NOESY (**10**-α): NOE correlation identified between H-4′ and H-2$_N$; H-4′ and H—H—6$_N$. *m/z* (ESI, α and β mixture) 358.0556 $[M-2H]^-$, $C_{11}H_{13}N_5O_7$ P requires 358.0558.

2″-Azido-2″-deoxyribo-NAD$^+$ (11). A mixture of **10** (0.0207 g, 0.046 mmol) and AMP-morpholidate (0.0183 g, 0.042 mmol) was co-evaporated with pyridine (3 × 2 mL) to remove residual water. Then $MgSO_4$ (0.010 g, 0.083 mmol) and $MnCl_2$ in formamide (313 μL, 0.063 mmol) were added under nitrogen. The reaction mixture was stirred at room temperature overnight under an atmosphere of nitrogen. The product was precipitated with acetonitrile and washed 2 × with acetonitrile. The precipitate was purified by ion-pair chromatography (0–50% methanol against 0.05 M TEAB-buffer pH 7.3 over 400 mL, flow rate 2 mL/min) and by ion exchange chromatography (0–100% 1 M TEAB buffer pH 7.3 against water over 400 mL, flow rate 2 mL/min) to give the product **11** as a colourless oil in 32% yield (1.02 equiv. Et_3N, 0.0106 g, 0.014 mmol). ^{1}H NMR (400 MHz, D_2O, **11**-β) δ_H 9.34 (s, 1H, H-2$_N$), 9.14 (d, J = 6.5 Hz, 1H, H-6$_N$), 8.82 (d, J = 8.0 Hz, 1H, H-4$_N$), 8.38 (s, 1H, H-8), 8.17 (dd, J = 6.5, 8.0 Hz, 1H, H-5$_N$), 8.10 (s, 1H, H-2), 6.07 (d, J = 5.5 Hz, 1H, H-1″), 5.99 (d, J = 6.0 Hz, 1H, H-1′), H-2′, H-3″ under water peak, 4.58 (apparent t, 1H, H-2″) 4.49–4.09 (m, 7H, H-3′, H-4′, H-4″, H-5$_{a,b}$′,H-5$_{a,b}$″). ^{13}C NMR (100 MHz, D_2O, **11**-β) δ_C 164.6 (q), 155.3 (C-8), 152.8 (C-2), 148.9 (q) 146.0 (C-4$_N$), 142.5 (C-6$_N$), 139.6 (C-2$_N$), 139.6 (q), 132.0 (q), 128.7 (C-5$_N$), 98.3 (C-1″), 87.0 (C-1′), 86.5 (C-4″), 83.7 (C-4′), 73.8 (C-2′), 70.7 (C-3′), 70.3 (C-3″), 68.1 (C-2″), 65.4 (C-5″), 64.4 (C-5′). ^{31}P NMR (162 MHz, D_2O, mix α and β) δ_P (-11.3) - (-11.8) (m). ^{1}H

NMR (400 MHz, D_2O, **11**-α) δ_H 9.05 (s, 1H, H-2_N), 8.89 (d, $J = 6.5$ Hz, 1H, H-6_N), 8.78 (d, $J = 8.0$ Hz,1H, H-4_N), 8.41 (s, 1H, H-8), 8.05 (s, 1H, H-2), 8.05–8.02 (m, 1H, H-5_N), 6.49 (d, $J = 6.1$ Hz, 1H, H-1″), 5.93 (d, $J = 6.1$ Hz, 1H, H-1′), 5.09–5.07 (m, 1H, H-2″),4.65 (apparent t, 1H, H-2′), H-3″ under water peak, 4.49–4.09 (m, 7H, H-3′, H-4′, H-4″, H-$5_{a,b}$′, H-$5_{a,b}$″). ^{13}C NMR (100 MHz, D_2O, **11**-α) δ_C 165.0 (q), 155.2 (C-8), 152.7 (C-2), 148.6 (q) 145.0 (C-4_N), 143.4 (C-6_N), 140.6 (C-2_N), 139.8 (q), 133.7 (q), 126.9 (C-5_N), 96.0 (C-1″), 88.1 (C-1′), 86.5 (C-4″), 83.7 (C-4′), 74.4 (C-2′), 71.0 (C-3′), 70.4 (C-3″), 65.5 (C-5″), 65.2 (C-5′), 64.1 (C-2″). *m/z* (ESI, α and β mixture) 687.1077 $[M-2H]^-$, $C_{21}H_{25}N_{10}O_{13}P_2$ requires 687.1083.

2″-Amino-2″-deoxyribo-NAD$^+$ (3). To a solution of **11** (0.0409 g, 0.047 mmol) in 10 mL water was added dithiothreitol (0.203 g, 1.31 mmol). The pH was adjusted to 7–8 with 0.1 M NaOH and the reaction was left stirring overnight. The solvent was reduced and the product was precipitated with ice-cold acetone to remove the dithiothreitol. The alpha and beta anomers were separated by semi-preparative HPLC (SAX column, 7 mM ammonium phosphate buffer pH 3.4) and the resulting inorganic phosphate was removed by subsequent RP chromatography (0–50% acetonitrile against water containing 0.01% trifluoroacetic acid) to give product **3** as the free acid in 57% combined yield of both anomers (**3**-α 0.0077 g, 0.012 mmol; **3**-β 0.0100 g, 0.015 mmol). ^{1}H NMR (400 MHz, D_2O, **3**-β, free acid) δ_H 9.51 (s, 1H, H-2_N), 9.36 (d, $J = 6.5$ Hz, 1H, H-6_N), 9.02–8.99 (m, 1H, H-4), 8.58 (s, 1H, H-8), 8.40 (s, 1H, H-2), 8.34 (dd, $J = 6.5$, 8.0 Hz, 1H, H-5_N), 6.66 (d, $J = 6.1$ Hz, 1H, H-1″), 6.14 (d, $J = 5.4$ Hz, 1H, H-1′), 4.86 (dd, $J = 2.8$, 5.8 Hz, 1H, H-3″), 4.72 (apparent t, 1H, H-2′), 4.68–4.65 (m, 1H, H-4″), 4.51–4.17 (m, 7H, H-2″, H-3′, H-4′, H-$5_{a,b}$′, H-$5_{a,b}$″). ^{13}C NMR (100 MHz, D_2O, **3**-β) δ_C 165.1 (C═O), 149.8 (q), 148.3 (q), 147.1 (C-4_N), 144.7 (C-2), 143.7 (C-6_N), 142.2 (C-8), 141.7 (C-2_N), 134.0 (q), 129.0 (C-5_N), 118.4 (q), 97.7 (C-1″), 87.8 (C-1′), 87.7 (C-4″), 84.0 (C-4′), 74.5 (C-2′), 70.1 (C-3′), 69.2 (C-3″), 65.1 (C-5″), 64.6 (C-5′), 58.4 (C-2″). NOESY (**3**-β): NOE correlation identified between H-1″ and H-4″; H-2″ and H-2_N; H-2″ and H-6_N. ^{31}P NMR (202 MHz, D_2O, **3**-β) δ −11.5 (d, $J_{p,p} = 20.7$ Hz), −11.2 (d, $J_{p,p} = 20.7$ Hz). *m/z* (neg ESI) 661.11774 $[M-2H]^-$, $C_{21}H_{27}N_8O_{13}P_2$ requires 661.11783; *m/z* (pos ESI) 663.13177 $[M]^+$, $C_{21}H_{29}N_8O_{13}P_2$ requires 663.13238. HPLC retention time 14.60 min (97.0%). TLC R_f 0.46 (isopropyl alcohol/H_2O/NH_4OH 6:3:1). ^{1}H NMR (400 MHz, D_2O, **3**-α, free acid) δ_H 9.40 (s, 1H, H-2_N), 9.20 (d, $J = 6.0$ Hz, 1H, H-6_N), 8.97 (d, $J = 8.0$ Hz, 1H, H-4_N), 8.57 (s, 1H, H-8), 8.36 (s, 1H, H-2), 8.26 (apparent t, 1H, H-5_N), 6.88 (d, $J = 6.1$ Hz, 1H, H-1″), 6.09 (d, $J = 5.5$ Hz, 1H, H-1′), 5.14–5.12 (m, 1H, H-4″), H-2′, H-2″, H-3″ under water peak, 4.51–4.49 (m, 1H, H-3′), 4.41–4-39 (m, 1H, H-4′), 4.25–4.17 (m, 4H, H-$5_{a,b}$′, H-$5_{a,b}$″). ^{13}C NMR (100 MHz, D_2O, **3**-α) δ_C 165.1(C═O), 150.6 (q), 148.3 (q), 146.3 (C-4_N), 145.8 (C-2), 144.2 (C-6_N), 141.9 (C-8), 141.9 (C-2_N), 133.7 (q), 128.4 (C-5_N), 118.4 (q), 96.7 (C-1″), 89.9 (C-4″), 87.6 (C-1′), 84.1 (C-4′), 74.5 (C-2′), 70.2 (C-3′), 69.7 (C-3″), 65.5 (C-5′), 65.2 (C-5″), 55.8 (C-2″). NOESY (**3**-α): NOE correlation identified between H-4″ and H-2_N; H-4″ and H-6_N. ^{31}P NMR (202 MHz, D_2O, **3**-α) δ_P −11.3. *m/z* (neg ESI) 661.11755 $[M-2H]^-$, $C_{21}H_{27}N_8O_{13}P_2$ requires 661.11783; *m/z* (pos ESI) 663.13184 $[M]^+$, $C_{21}H_{29}N_8O_{13}P_2$ requires 663.13238. HPLC retention time 13.90 min (95.4%). TLC R_f 0.48 (isopropyl alcohol/H_2O/NH_4OH 6:3:1).

5.3. Biochemical evaluation

Sirtuin assay. The sirtuin inhibition assay was carried out in 96-well plates (OptiPlate™-96F, PerkinElmer) Sirtuin-buffer (50 mM Tris/HCl, 137 mM NaCl, 2.7 mM KCl) (17 μL), SIRT1, SIRT2 or SIRT3 solution (0.5 Units, 30 μL), DMSO(3 μL, assay concentration 8.3% (v/v)), ZMAL (5 μL, assay concentration 10.5 μM), β-NAD$^+$ (5 μL, assay concentration 500 μM) and the NAD$^+$ analogues as potential sirtuin inhibitors were mixed in a 96-well microplate. After incubation for 4 h at 37 °C (500 rpm, Heidolph Inkubator 1000) a trypsin containing stop solution (5.5 U/μL trypsin, 8 mM nicotinamide, 100 mM NaCl, 50 mM Tris, 6.7% (v/v), DMSO, pH 8.0, 60 μL) was added and the samples were incubated for another 20 min at 37 °C. Afterwards fluorescence was measured with a POLARstar Optima Microplate reader (BMG Labtech, Offenburg).

For the substrate assay, the 2″–NH_2 NAD$^+$ analogues (500 μM) were used instead of natural β-NAD$^+$.

ADP-ribosylation assay. In-vitro ADP-ribosylation of actin was performed using 1 μM of purified α-skeletal muscle actin, 1 μM NAD$^+$ and radioactive [^{32}P]NAD$^+$ (0.5 μCi per sample) in G buffer (5 mM Tris-HCl, 0.2 mM $CaCl_2$, 0.2 mM ATP and 0.5 mM dithiothreitol (DTT), pH 8.0). Samples were pre-incubated with different concentrations of 2″–NH_2 *ribo* β-NAD$^+$ or 2″–NH_2 *arabino* β-NAD$^+$ for 15 min at 21 °C, before ADP-ribosylation was started with the addition of 70 nM of TccC3hvr from *Photorhabdus luminescens*. After 6 min at 21 °C, samples were then subjected to SDS-PAGE (12.5% SDS) followed by autoradiography.

5.4. Stability measurements

Sirtuin buffer. Deionised water containing 50 mM Tris/HCl, 137 mM NaCl, 2.7 mM KCl, adjusted to pH 8.0 with 1 M NaOH.

Sample preparation. 10 mM stock solutions of 2″–NH_2 *ribo* α-/β-NAD$^+$ were prepared in sirtuin-buffer. For the stability tests in only buffer, the samples were diluted to a final concentration of 1 mM with sirtuin-buffer pH 8.0. For tests including SIRT2 and Z-(Ac)Lys-AMC (ZMAL), ZMAL was added in a final concentration of 10.5 μM (126 μM stock solution in DMSO) and 5 μL SIRT2 (SW156515, 1.0 mg/mL) were added to each sample. The samples were incubated at 37 °C on a Titramax 1000 Vibrating Platform Shaker from Heidolph. HPLC samples were analysed after 0, 1, 2, 3, 4 h. The samples were vortexed prior HPLC analysis using a Heidolph REAX Top Vortexer. For generation of the calibration curve, nicotinamide (Sigma-Aldrich) was dissolved in deionised water and samples of different concentration from 0.12 mM to 9.87 mM were analysed by HPLC.

HPLC conditions. The stability experiments were analysed by high performance liquid chromatography (HPLC) on an Agilent 1200 series equipped with a diode array detector (detection wavelength 254 nm). The samples were analysed on a Supelcosil™ LC-18 column (250 × 4.6 mm, particle size 5 μm, pore size 120 Å, Sigma-Aldrich) using a mobile phase composed of 0.05 M KH_2PO_4 buffer pH 6.0 (solvent A) and acetonitrile/buffer 1:1 (solvent B) according to the gradient shown in Table 5. Injection volume: 10 μL (volume in HPLC vial: 15 μL). A blank sample containing only buffer was recorded for baseline correction.

5.5. Computational methods

Protein structures of SIRT2 in complex with NAD$^+$ or carba-NAD$^+$ (PDB IDs: 4RMG, 5DY4, 5G4C, 4X3P) and of SIRT1 in complex with ADPR (PDB ID: 4KXQ) were downloaded from the Protein Data Bank. All protein structures were prepared by using the Structure Preparation module in MOE. Hydrogen atoms were added, for titratable amino acids the protonation state was calculated using the Protonate 3D module in MOE. Protein structures were energy minimized using the AMBER12-EHT force field[41] using a tethering force constant of (3/2) kT/2 (σ = 0.5 Å) for all atoms during the minimization. AM1-BCC charges[42] were used for ligands. All molecules except the zinc ion were removed from the structures.

Protein-ligand docking was performed using program GOLD 5.2.[43] Phe96 was used to define the size of the grid box for SIRT2 (15 Å radius).

Table 5
HPLC gradient for stability experiments.

Time [min]	*Solvent A [%]*	*Solvent B [%]*
0	100	0
8	100	0
20	0	100
24	0	100
30	100	0

Water molecules that were found to bridge the interaction between SIRT2 and NAD^+ were considered using the toggle-option within GOLD (water molecules are allowed to be displaced by the ligand). The ligands were treated as flexible and 100 docking poses were calculated for each ligand using Goldscore as scoring function. The top-ranked poses from each docking run were included in the final analysis and were refined using the MM-GB/SA option and the AMBER12EHT force field in MOE. During the minimization protein backbone atoms were tethered using a force constant of (3/2) kT/2 ($\sigma = 0.5$ Å). Complexes showing the lowest binding free energy value were selected for each inhibitor. Using this docking setup, NAD^+ as well as carba-NAD^+ co-crystallized with SIRT2 could be correctly docked into the crystal structure with RMSD between 0.80 and 1.7 Å. The best docking solution was obtained for NAD^+ co-crystallized in the SIRT2 structure 5DY4.

Declaration of Competing Interest

The authors declare that they have no known competing financial interests or personal relationships that could have appeared to influence the work reported in this paper.

Acknowledgement

Financial support by the German Academic Exchange Service (DAAD), King's College London, the University of Freiburg, the European Union's Seventh Framework Programme for research, technological development and demonstration under grant agreement number 602080 (A-ParaDDisE), and the Deutsche Forschungsgemeinschaft (AK6/22-2; Ju295/14-1; INST 39/931-1) is gratefully acknowledged. We thank the EPSRC National Mass Spectrometry Facility for the recording of mass spectra.

Appendix A. Supplementary material

Supplementary data to this article can be found online at https://doi.org/10.1016/j.bmc.2022.116875.

References

1 Barrio JR, Secrist JA, Leonard NJ. A Fluorescent Analog of Nicotinamide Adenine Dinucleotide. *Proc Natl Acad Sci USA*. 1972;69:2039–2042.
2 Pergolizzi G, Butt JN, Bowater RP, Wagner GK. A novel fluorescent probe for NAD-consuming enzymes. *Chem Commun*. 2011;47:12655–12657.
3 Gibson BA, Zhang Y, Jlang H, et al. Chemical Genetic Discovery of PARP Targets Reveals a Role for PARP-1 in Transcription Elongation. *Science*. 2016;353(6294):45–50.
4 Jiang H, Kim JH, Frizzell KM, Kraus WL, Lin H. Clickable NAD Analogues for Labeling Substrate Proteins of Poly(ADP-ribose) Polymerases. *J Am Chem Soc*. 2010;132:9363–9372.
5 Wang Y, Fung YME, Zhang W, et al. Deacylation Mechanism by SIRT2 Revealed in the 1′-SH-2′-O-Myristoyl Intermediate Structure. *Cell Chem Biol*. 2017;24:339–345.
6 Lin H. Nicotinamide adenine dinucleotide: beyond a redox coenzyme. *Org Biomol Chem*. 2007;5:2541–2554.
7 Belenky P, Bogan KL, Brenner C. NAD^+ metabolism in health and disease. *Trends Biochem Sci*. 2007;32:12–19.
8 Chen B, Zang W, Wang J, et al. The chemical biology of sirtuins. *Chem Soc Rev*. 2015;44:5246–5264.
9 Jing H, Lin H. Sirtuins in Epigenetic Regulation. *Chem Rev*. 2015;115:2350–2375.
10 Hu J, Jing H, Lin H. Sirtuin inhibitors as anticancer agents. *Future Med Chem*. 2014;6:945–966.
11 Imai S, Armstrong CM, Kaeberlein M, Guarente L. Transcriptional silencing and longevity protein Sir2 is an NAD-dependent histone deacetylase. *Nature*. 2000;403:795–800.
12 Feldman JL, Baeza J, Denu JM. Activation of the protein deacetylase SIRT6 by long-chain fatty acids and widespread deacylation by mammalian sirtuins. *J Biol Chem*. 2013;288:31350–31356.
13 Du J, Zhou Y, Su X, et al. Sirt5 is a NAD-dependent protein lysine demalonylase and desuccinylase. *Science*. 2011;334:806–809.
14 Feige JN, Auwerx J. Transcriptional targets of sirtuins in the coordination of mammalian physiology. *Curr Opin Cell Biol*. 2008;20:303–309.
15 Verdin E, Hirschey MD, Finley LW, Haigis MC. Sirtuin regulation of mitochondria: energy production, apoptosis, and signaling. *Trends Biochem Sci*. 2010;35:669–675.
16 Liu TF, Vachharajani VT, Yoza BK, McCall CE. NAD^+-dependent sirtuin 1 and 6 proteins coordinate a switch from glucose to fatty acid oxidation during the acute inflammatory response. *J Biol Chem*. 2012;287:25758–25769.
17 Haigis MC, Guarente LP. Mammalian sirtuins–emerging roles in physiology, aging, and calorie restriction. *Genes Dev*. 2006;20:2913–2921.
18 Du J, Jiang H, Lin H. Investigating the ADP-ribosyltransferase activity of sirtuins with NAD analogues and ^{32}P-NAD. *Biochemistry*. 2009;48:2878–2890.
19 Sleath PR, Handlon AL, Oppenheimer NJ. Pyridine coenzyme analogs. 3. Synthesis of three NAD^+ analogs containing a 2'-deoxy-2'-substituted nicotinamide arabinofuranosyl moiety. *J Org Chem*. 1991;56:3608–3613.
20 Cen Y, Sauve AA. Diastereocontrolled Electrophilic Fluorinations of 2-Deoxyribonolactone: Syntheses of All Corresponding 2-Deoxy-2-fluorolactones and 2"-Deoxy-2"-fluoro-NAD^+s. *J Org Chem*. 2009;74:5779–5789.
21 Pesnot T, Kempter J, Schemies J, et al. Two-step synthesis of novel, bioactive derivatives of the ubiquitous cofactor nicotinamide adenine dinucleotide (NAD). *J Med Chem*. 2011;54:3492–3499.
22 Pergolizzi G, Cominetti MM, Butt JN, Field RA, Bowater RP, Wagner GK. Base-modified NAD and AMP derivatives and their activity against bacterial DNA ligases. *Org Biomol Chem*. 2015;13:6380–6398.
23 Handlon AL, Xu C, Muller-Steffner HM, Schuber F, Oppenheimer NJ. 2'-Ribose Substituent Effects on the Chemical and Enzymic Hydrolysis of NAD^+. *J Am Chem Soc*. 1994;116:12087–12088.
24 Guse AH, Cakir-Kiefer C, Fukuoka M, et al. Novel hydrolysis-resistant analogues of cyclic ADP-ribose: modification of the "northern" ribose and calcium release activity. *Biochemistry*. 2002;41:6744–6751.
25 Cakir-Kiefer C, Muller-Steffner H, Oppenheimer N, Schuber F. Kinetic competence of the cADP-ribose-CD38 complex as an intermediate in the CD38/NAD^+ glycohydrolase-catalysed reactions: implication for CD38 signalling. *Biochem J*. 2001;358:399–406.
26 Liang CW, Kim MJ, Jeong LS, Chun MW. Synthesis of 2-(3'-azido- and 3'-amino-3'-deoxy-beta-D-ribofuranosyl)thiazole-4-carboxamide. *Nucleosides Nucleotides Nucleic Acids*. 2003;22:2039–2048.
27 Ikehara M, Uesugi S, Yoshida K. Nucleosides and nucleotides. XLVII. Conformation of purine mucleosides and their 5'-phosphates. *Biochemistry*. 1972;11:830–836.
28 Sarma RH, Lee CH, Evans FE, Yathindra N, Sundaralingam M. Probing the interrelation between the glycosyl torsion, sugar pucker, and the backbone conformation in C(8) substituted adenine nucleotides by ^{1}H and ^{1}H-(^{31}P) fast Fourier transform nuclear magnetic resonance methods and conformational energy calculations. *J Am Chem Soc*. 1974;96:7337–7348.
29 Handlon AL, Oppenheimer NJ. Substituent effects on the pH-independent hydrolysis of 2'-substituted nicotinamide arabinosides. *J Org Chem*. 1991;56:5009–5010.
30 Heltweg B, Trapp J, Jung M. In vitro assays for the determination of histone deacetylase activity. *Methods*. 2005;36:332–337.
31 Lang AE, Schmidt G, Schlosser A, et al. Photorhabdus luminescens toxins ADP-ribosylate actin and RhoA to force actin clustering. *Science*. 2010;327:1139–1142.
32 Feldman JL, Dittenhafer-Reed KE, Kudo N, et al. Kinetic and structural basis for acyl-group selectivity and NAD^+-dependence in Sirtuin-catalyzed deacylation. *Biochemistry*. 2015;54(19):3037–3050.
33 Davenport AM, Huber FM, Hoelz A. Structural and Functional Analysis of Human SIRT1. *J Mol Biol*. 2014;426:526–541.
34 Schiedel M, Rumpf T, Karaman B, et al. Aminothiazoles as Potent and Selective Sirt2 Inhibitors: A Structure-Activity Relationship Study. *J Med Chem*. 2016;59:1599–1612.
35 Bitterman KJ, Anderson RM, Cohen HY, Latorre-Esteves M, Sinclair DA. Inhibition of silencing and accelerated aging by nicotinamide, a putative negative regulator of yeast sir2 and human SIRT1. *J Biol Chem*. 2002;277:45099–45107.
36 Schmidt MT, Smith BC, Jackson MD, Denu JM. Coenzyme specificity of Sir2 protein deacetylases: implications for physiological regulation. *J Biol Chem*. 2004;279:40122–40129.
37 Sauve AA, Schramm VL. Sir2 regulation by nicotinamide results from switching between base exchange and deacetylation chemistry. *Biochemistry*. 2003;42:9249–9256.
38 Jackson MD, Schmidt MT, Oppenheimer NJ, Denu JM. Mechanism of nicotinamide inhibition and transglycosidation by Sir2 histone/protein deacetylases. *J Biol Chem*. 2003;278:50985–50998.
39 Rye PT, Frick LE, Ozbal CC, Lamarr WA. Advances in label-free screening approaches for studying sirtuin-mediated deacetylation. *J Biomol Screen*. 2011;16:1217–1226.
40 Guan X, Lin P, Knoll E, Chakrabarti R. Mechanism of Inhibition of the Human Sirtuin Enzyme SIRT3 by Nicotinamide: Computational and Experimental Studies. *PLoS ONE*. 2014;9:e107729.
41 Wang J, Wolf RM, Caldwell JW, Kollman PA, Case DA. Development and Testing of a General Amber Force Field. *J Comput Chem*. 2004;25:1157–1174.
42 Jakalian A, Jack DB, Fast BCI. Efficient Generation of High-quality Atomic Charges. AM1-BCC Model: II. Parameterization and Validation. *J Comput Chem*. 2002;23:1623–1641.
43 Jones G, Willett P, Glen RC, Leach AR, Taylor R. Development and validation of a genetic algorithm for flexible docking. *J Mol Biol*. 1997;267:727–748.